














Experimental and computational investigation of reduced graphene oxide nanoplatelets stabilized in poly(styrene sulfonate) sodium salt

Celina M. Miyazaki^{1,2} , Marco A. E. Maria^{1,3,4} , Daiane Damasceno Borges⁴ , Cristiano F. Woellner⁴ , Gustavo Brunetto⁴ , Alexandre F. Fonseca⁴ , Carlos J. L. Constantino⁵ , Marcelo A. Pereira-da-Silva^{6,7} , Abner de Siervo⁴ , Douglas S. Galvao⁴ , and Antonio Riul Jr.^{4,*} 

¹ POSMAT – Programa de Pós-Graduação em Ciência e Tecnologia de Materiais, UNESP – Univ Estadual Paulista, Bauru, SP, Brazil

² Universidade Federal de São Carlos – DFQM, Sorocaba, SP, Brazil

³ Faculdade de Engenharia de Sorocaba – FACENS, Sorocaba, SP, Brazil

⁴ Applied Physics Department, State University of Campinas, Campinas, SP 13083-970, Brazil

⁵ UNESP – Univ Estadual Paulista, Presidente Prudente, SP, Brazil

⁶ Centro Universitário Central Paulista – UNICEP, São Carlos, SP, Brazil

⁷ Instituto de Física de São Carlos – USP, São Carlos, SP, Brazil

Received: 31 January 2018

Accepted: 12 April 2018

Published online:

19 April 2018

© Springer Science+Business Media, LLC, part of Springer Nature 2018

ABSTRACT

The production of large-area interfaces and the use of scalable methods to build up designed nanostructures generating advanced functional properties are of high interest for many materials science applications. Nevertheless, large-area coverage remains a major problem even for pristine graphene, and here we present a hybrid, composite graphene-like material soluble in water that can be exploited in many areas such as energy storage, electrodes fabrication, selective membranes and biosensing. Graphene oxide (GO) was produced by the traditional Hummers' method being further reduced in the presence of poly(styrene sulfonate) sodium salt (PSS), thus creating stable reduced graphene oxide (rGO) nanoplatelets wrapped by PSS (GPSS). Molecular dynamics simulations were carried out to further clarify the interactions between PSS molecules and rGO nanoplatelets, with calculations supported by Fourier transform infrared spectroscopy analysis. The intermolecular forces between rGO nanoplatelets and PSS lead to the formation of a hybrid material (GPSS) stabilized by van der Waals forces, allowing the fabrication of high-quality layer-by-layer (LbL) films with poly(allylamine hydrochloride) (PAH). Raman and electrical characterizations corroborated the successful modifications in the electronic structures from GO to GPSS after the chemical treatment, resulting in (PAH/GPSS) LbL films four orders of magnitude more conductive than (PAH/GO).

Address correspondence to E-mail: riul@ifi.unicamp.br

Introduction

Graphene is a milestone in carbon-based and 2D soft materials due to its unique mechanical, thermal, electrical and optical properties, which led to a myriad of experimental and theoretical studies and applications in energy [1–3], sensing [4], devices [5, 6] and the production of hybrid materials featuring new properties [7]. It is a one-atom thick sheet made of sp^2 carbons arranged in a honeycomb lattice that was first obtained by mechanical exfoliation of pyrolytic graphite [8]. Even considering recent advances in chemical synthesis methods [9], the production of high-quality large-area graphene is still challenging.

Chemical synthesis is an alternative approach enabling a moderate fabrication of graphene-based materials under mild conditions, with added benefits of functionalization that allows the formation of hybrids or composites with polymers, nanoparticles, DNA, etc. [10]. Usually, the chemical process begins with graphite exfoliation by the Hummers' method [11], generating graphene oxide (GO), an insulating material with functional oxygen groups on the basal planes and at the edges of the formed nanoplatelets. The oxidation process makes GO easily dissolved in water, and it can be further processed to reduced graphene oxide (rGO), which is a more conductive material resembling the graphene properties. The highest observed conductivity in rGO is explained by the partial reestablishment of the carbon sp^2 network after the chemical reduction process [12, 13], and despite being less conductive than pristine graphene, rGO is an attractive material for interfacial applications [14].

The use of graphene-based materials usually requires the deposition on a solid substrate such as silicon, quartz or glass. Within this context, the layer-by-layer (LbL) technique is an alternative and versatile way to promote graphene-functionalized surfaces as it allows for well-defined molecular-level control over thickness, morphology and structure, designing advanced functional nanostructures in a diverse range of applications onto practically any surface [15]. LbL films of graphene derivatives have been widely used in energy [16, 17], selective membranes [18, 19], sensing and biosensing [4, 20, 21] applications.

There is a plethora of studies with LbL films of graphene-based materials, such as composites with polymers used in electromagnetic interference shielding at GHz range [22]. Lee and co-workers [23] achieved transparent, conducting LbL films using chemically modified rGO with controlled thickness, and different three-dimensional GO structures could be formed throughout a new diffusion-driven layer-by-layer assembly process [24]. Multi-walled carbon nanotubes and rGO composites were employed in point-of-care and clinical screening of multiple diseases [25], and the assembly of carbon nanomaterials with conducting polymers was used to build up 3D nanoarchitectures for energy storage and sensing applications [26]. Since the LbL assembly is based on the spontaneous adsorption of material from aqueous suspensions [15, 27, 28], it is of great importance the development, synthesis and characterization of water-soluble graphene-based materials that can be further studied in distinct applications.

In this work, we present the chemical synthesis and characterization of rGO nanoplatelets functionalized with sodium polystyrene sulfonate (PSS), a water-soluble material called here as GPSS. Molecular dynamics (MD) simulations were carried out to provide further insights into the self-organization of GPSS structure. It forms stable suspensions in water for ~ 10 weeks, and it is attractive for LbL assemblies, expanding the possibility of applications in energy conversion, barrier properties, sensing and biosensing by the fact that pristine rGO is poorly dispersed in several known solvents. Fourier transform infrared spectroscopy (FTIR) analysis helped to identify the role played by van der Waals interactions between PSS and rGO nanoplatelets in the formed GPSS nanostructure. Poly(allylamine hydrochloride) (PAH) was used as a positively charged polyelectrolyte to build up both (PAH/GO) and (PAH/GPSS) LbL nanostructures with controlled thickness and morphology. Measurements taken by atomic force microscope (AFM) indicated the presence of larger GO nanoplatelets when compared to GPSS, and impedance characterization shows that the (PAH/GPSS) film is four orders of magnitude more conductive than (PAH/GO), thus confirming the efficacy of the reduction process in the GPSS formation.

Materials and methods

Materials

Graphite powder (98%), H₂SO₄ (95%), KMnO₄ (99%), K₂S₂O₈ (99%), P₂O₅, H₂O₂, H₆N₂O₄S were of analytical grade and used in the synthesis processes. Poly(styrene sulfonate) sodium salt—PSS (Mw = ~ 70000), and poly(allylamine hydrochloride)—PAH (Mw ~ 15000), were purchased from Sigma-Aldrich and used as received. Ultrapure water (18.2 MΩ cm) acquired from a Millipore Direct Q5 system (at 25 °C) was used in all experiments.

GO and GPSS nanoplatelets synthesis

A pre-oxidation process of graphite was performed in accordance with Kovtyukhova et al. [29] in which graphite (10 g) was immersed in a mixture of concentrated H₂SO₄ (15 mL), K₂S₂O₈ (5 g) and P₂O₅ (5 g) at 80 °C, reacting for 6 h at room temperature. Water was carefully added to dilution, and the solid was washed till neutral pH. Sequentially, the Hummers' method [11, 29] was applied by adding 10 g of pre-oxidized graphite into concentrated H₂SO₄ (230 mL) (cold bath at 0 °C). 30 g KMnO₄ was added slowly with constant stirring with extreme caution as the temperature should not exceed 20 °C. The mixture was stirred for 2 h at 35 °C. Water (460 mL) was added and allowed to react for 15 min, and then, 1.4 L of water and 30% H₂O₂ (25 mL) were added to stop the reaction. The resulting yellow product was filtered, washed with 1:10 HCl solution and dried in vacuum oven at room temperature to produce GO.

For the GPSS synthesis, PSS and GO were added according to Stankovich et al. [30]. Briefly, 50 mL of GO suspension (1 g L⁻¹) was prepared in ultrasonic bath for 30 min and mixed with 500 mg of PSS. The mixture was kept under vigorous stirring, and hydrazine sulfate was added to a final concentration of 0.01 mol L⁻¹. The final product (GPSS) was stirred and maintained at 90 °C for 12 h, being further washed with ultrapure water and dried at 90 °C in vacuum oven. GPSS was characterized with UV–Vis absorption spectroscopy using a Thermo Scientific Genesys 6 equipment, while Raman spectroscopy was performed with a micro-Raman Renishaw, model in-Via, laser at 633 nm. FTIR spectroscopy was acquired in a Thermo Nicolet, model Nexus 470. The chemical composition of the samples was analyzed

by X-ray photoelectron spectroscopy (XPS) in a homemade setup using a vacuum chamber (10 mbar) and Mg K α radiation (1253.6 eV) with 240 W. Shirley background was assumed to the XPS spectra fitting. Electrical measurements were acquired in a homemade four-probe setup in accordance with Ref [31], using drop-cast films of GO and GPSS deposited on quartz substrates, with film thickness measured by a Veeco Dektak 150 surface profilometer.

Molecular Dynamics Simulations

Molecular dynamics (MD) simulations were carried out to study the rGO nanoplatelets wrapped by PSS and water molecules. The preparation of the initial configuration of the system consisted in randomly placing PSS and water molecules around one single rGO nanoplatelet. PSS was built with 16 monomers of sulfonated styrene group (see Fig. 1). Every sulfonate group is treated as fully ionized, and Na⁺ was added to neutralize the system. The water content is 5 water molecules per sulfonate groups. The rGO sheet has dimensions of ~ 40 × 40 Å (~ 1600 Å² in area), with the atomic concentration of the functional group

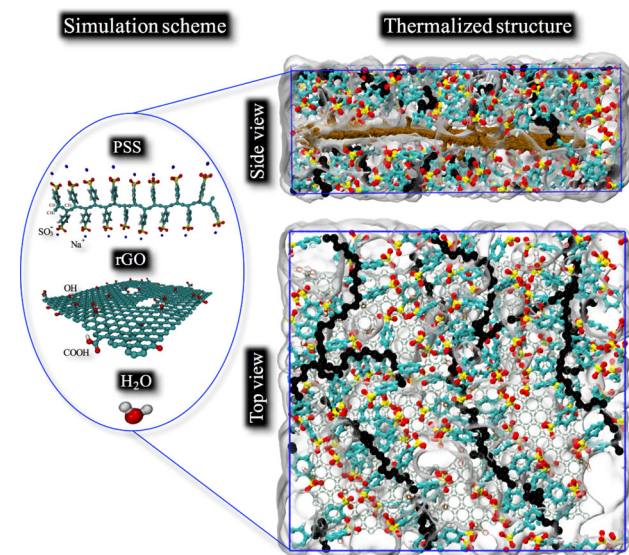


Fig. 1 In the left side, it shows the simulation system components and, in the right, a snapshot of the thermalized GPSS structure. The PSS backbone and aromatic rings united atoms are represented by black and cyan colors, while the terminated SO₃⁻ atoms are in yellow and red colors. The rGO nanoplatelet is in brown color, and the water is represented in a continuum transparent surface. The thermalized structure clearly shows PSS being in stretched conformation with the sulfonated styrene groups “lying” on rGO.

been 2% hydroxyl, 2% epoxy, 1% carboxyl and 1% carbonyl. The functional group percentages are based on the XPS data discussed along this manuscript. The hydroxyl and epoxy groups are situated away from the edges, while carboxyl and carbonyl groups are on the boundaries of the nanoplatelets [32, 33], as shown in Fig. 1. Once the initial configuration was set, the system was equilibrated after a series of annealing and optimization runs using Berendsen thermostat and barostat [34]. After equilibration at ambient temperature and pressure (i.e., $T = 300$ K and $P = 1$ atm), canonical trajectories of 2 ns using Nosé–Hoover integrator scheme [35, 36] were generated for analysis.

The pair-atom interactions were described within the classical formalism. Water molecules were described by rigid 3-sites Transferable Intermolecular Potential (TIP-3P) [37] model. To simulate the rGO nanoplatelets, all atoms were considered explicitly in the simulations (*all-atom* approach), whereas a mixed representation was used to describe the PSS molecule. The united atom model was used to describe the backbone chain, while all atomistic representation was applied to describe benzene ring and sulfonate groups. The force field parameters including bonded and non-bonded interactions for the PSS were extracted from Ref. [38], while for the rGO were extracted from Ref. [39]. The initial configuration was built using Packmol [40], and the MD simulations were carried out using LAMMPS [41].

LbL films assembly and characterization

LbL films were fabricated using PAH as positive polyelectrolyte (1 mg mL^{-1}) for both GO and GPSS, which were used as negatively charged suspensions (0.1 mg mL^{-1}), thus forming $(\text{PAH/GO})_n$ and $(\text{PAH/GPSS})_n$ multilayers, being n the number of deposited bilayers. All solutions were adjusted to pH 3.5, including those for washing. The immersion time was equal to 3 min for PAH and 5 min for GO and GPSS solutions. The LbL film fabrication was made using an automated dipper from a Langmuir trough (NIMA Technology, model 612D), with upward and downward rates of 60 and 10 mm min^{-1} , respectively.

LbL films were characterized using UV–Vis spectroscopy (Thermo Scientific Genesys 6), AFM (Bruker Dimension ICON Nanoscope-V) at intermittent contact mode with a silicon cantilever (40 N/m ,

330 kHz), and impedance measurements (Solartron impedance analyzer 1260A, coupled to a 1296 Dielectric Interface) were acquired from 1 MHz to 1 Hz , using 20 mV amplitude. $(\text{PAH/GO})_5$ and $(\text{PAH/GPSS})_5$ LbL films were deposited onto gold interdigitated electrodes (IDEs) having 30 pairs of digits, 3 mm long, $40 \mu\text{m}$ width and separated $40 \mu\text{m}$ each other. The IDEs were fabricated at the Brazilian Nanotechnology National Laboratory (LNNano/CNPEM—Campinas, Brazil).

Results and discussion

GO and GPSS aqueous dispersions were characterized by UV–Vis absorption spectroscopy (Figure S1), displaying bands at 229 and 282 nm , characteristic of π – π^* transition of aromatic C–C bond, and n – π^* transition of C=O bond, respectively [42, 43]. GPSS solution presents a band at 268 nm due to π – π^* transition (shifted to higher wavelength), suggesting that the electronic sp^2 conjugation was restored [42], and a band at 227 nm due to the PSS benzene group absorption [44]. The dispersions were stable for ~ 10 weeks, demonstrating that rGO is effectively dispersed in water with the presence of PSS.

Figure 2 presents the Raman spectra of powder samples from graphite, GO, pristine rGO and GPSS. The G-band at $\sim 1590 \text{ cm}^{-1}$ from the E_{2g} degenerate mode zone vibration [45] of the sp^2 carbon network, and the D-band at $\sim 1330 \text{ cm}^{-1}$ attributed to defects

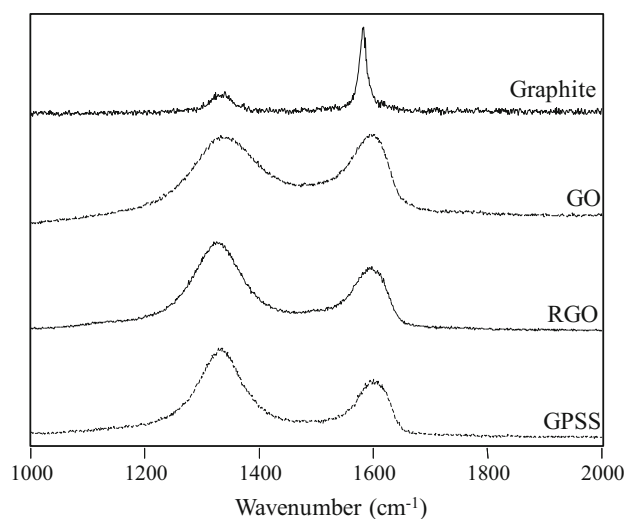


Fig. 2 Raman spectra of graphite, GO, rGO and GPSS powder samples.

in the sp^2 carbon lattice were investigated [46, 47]. D and G peak positions were only slightly shifted to higher wavenumbers (see Table 1) comparing pristine rGO with GPSS, suggesting that PSS is not chemically bonded to rGO sheet, consequently not affecting the sp^2 network domains. The I_D/I_G ratio increased after the GO reduction to form both rGO and GPSS, suggesting a decreased average size of the sp^2 carbon domains [48, 49], which means that new sp^2 domains were created, however, smaller in size and more numerous than those present in GO.

The atomic ratio of C and O was obtained from XPS survey spectra (Figure S2) indicating a successful reduction process by the decrease in O/C ratio from 51.4 to 7% [13]. Figure 3 shows the high-resolution C1s XPS analysis of GO and GPSS, with C=C bonds increasing from 48.7 to 74.3% after the chemical reduction. The GO spectrum indicates high degree of oxidation with three main components: C–C from non-oxygenated ring (284.5 eV), C in C–O bonds (286.6 eV) and C in C=O from carbonyl groups (288.5 eV). The GPSS spectrum indicated a marked decrease in the oxygenated groups and an additional peak at ~ 285 eV related to C–S from PSS [50]. Table 2 presents the relative percentage of each functional group, which is an important data for the computational analysis.

FTIR analysis (Figure S3) indicated typical GO bands at 1626 cm^{-1} (C=C stretching), and the presence of oxy-groups at 1739 cm^{-1} (C=O stretching), 1057 cm^{-1} (C–O stretching), 1405 cm^{-1} (C=OH stretching) and 1225 cm^{-1} (epoxy group) [51], with a broad absorption band at $\sim 3400\text{ cm}^{-1}$ (C–OH stretching) [52]. After the reduction process with hydrazine and PSS, the oxy-group bands disappeared, while a comparison between PSS with GPSS spectra shows a shift in the benzene ring vibration in PSS from 1128 to 1132 cm^{-1} , indicative of physical interactions between PSS and the rGO, hampering

Table 1 Raman spectroscopy data for graphite, GO, rGO and GPSS powder samples

	D peak position	G peak position	I_D/I_G^a
Graphite	1335	1582	0.27 ± 0.01
GO	1336	1596	0.96 ± 0.02
rGO	1325	1596	1.34 ± 0.05
GPSS	1331	1599	1.41 ± 0.11

^a I_D/I_G calculated as average of 5 measurements

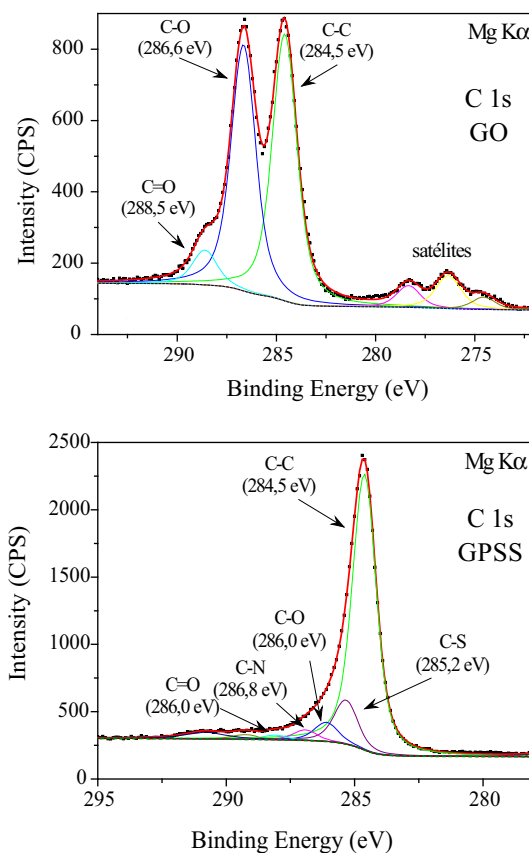


Fig. 3 XPS spectra for GO and GPSS in the region of C1s.

the vibrations of the PSS chains. The observed shift in the FTIR spectra can be related to a strong interaction between PSS molecules and rGO nanoplatelets.

In order to better understand the GPSS structure, classical MD simulations were performed. Figure 1 shows a typical snapshot of the self-organized system containing PSS, water and rGO well thermalized at ambient temperature and pressure. The typical mass density is approximately 1.4 g/cm^3 , which is higher than 0.8 g/cm^3 PSS in bulk. Figure 4a shows the radial distribution function between oxygen atoms of the sulfonate groups and hydrogen of OH and COOH functional groups. The simulations reveal that the PSS interacts with rGO mainly through the hydroxyl and carboxyl groups forming H-bonds (see Fig. 4). Moreover, the water molecules intermediate this interaction also via H-bonds as shown in RDF of water–functional group water– SO_3^- presented in Fig. 4b. The PSS is found in stretched conformation with the sulfonated styrene groups “lying” on rGO (see Fig. 1). This conformation maximizes the SO_3^- –OH interactions and minimizes the electrostatic repulsion among sulfonate neighbors. This

Table 2 Relative percentage of functional groups to GO and GPSS samples

Sample	Functional group	%	Sample	Functional group	% ^a
GO	C=C (sp ² network)	48.7	GPSS	C=C (sp ² network)	74.3
	C–O	44.9		C–S	11.8
	C=O	6.5		C–O	5.2
		O–C=O		1.3	
				C=O	1.2

^aGPSS spectrum presented 2.8% signal from C in impurities and 3.4% from π - π^* satellite

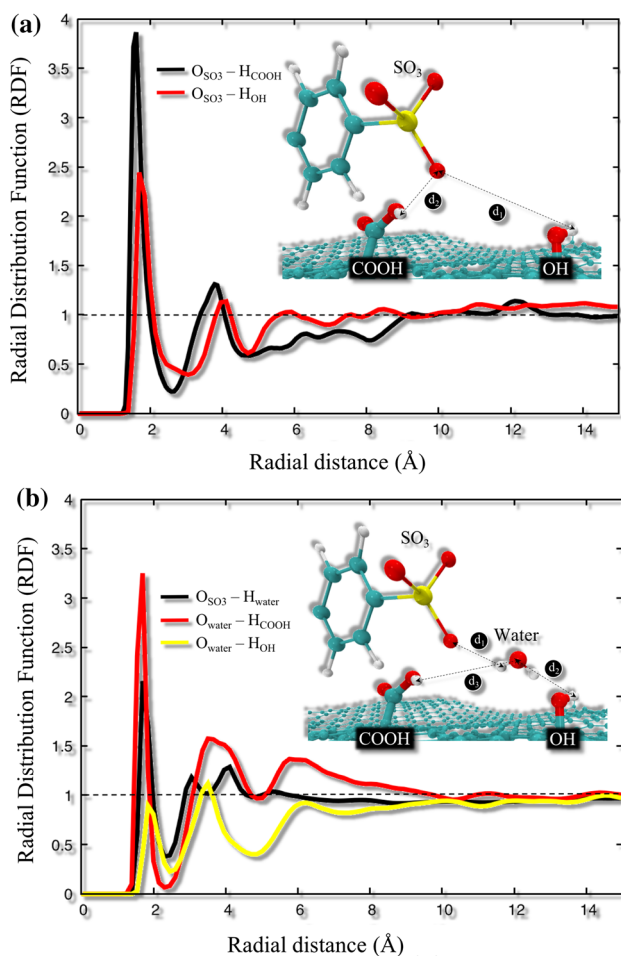


Fig. 4 Radial pair distribution function, $g(r)$, of oxygen atoms in the PSS molecule (a) and hydrogen atoms in carboxylic groups (b) of the rGO nanoplatelet.

interaction should be strong enough to trap the styrene groups and, thus, hamper the vibration of PSS chain as suggested by FTIR analysis. These results are in good agreement with Raman studies [53], indicating that there is a trend to PSS accommodation close to rGO nanoplatelet without chemical interaction.

DC measurements acquired from the four-probe technique (see Figure S6) indicated conductivity values of $2.0 \times 10^{-2} \text{ S cm}^{-1}$ for GO and $6.3 \times 10^2 \text{ S cm}^{-1}$ for GPSS, similar to values in the literature [42, 54] and lower than those found for printed pristine graphene ($\sim 2.5 \times 10^4 \text{ S cm}^{-1}$) [55]. This difference can be explained by defects and residual oxygen containing groups remaining in the rGO nanoplatelets from the chemical reduction process [14], remarkably impacting the electrical properties of GPSS when compared to pristine graphene. Nevertheless, our results corroborate the information of better electronic properties for GPSS when compared to GO [56] due to a better reestablishment of the sp² carbon network in the formed rGO nanoplatelets, which is not disturbed owing to the non-covalent interactions between PSS molecules, in close agreement with the MD simulation, Raman and FTIR analysis.

After characterization of GPSS and GO, PAH polyelectrolyte was used to build up both (PAH/GO) and (PAH/GPSS) LbL nanostructures. LbL film growth was investigated using UV–Vis absorption spectroscopy, as shown in Fig. 5. It was initially determined the best immersion time in each polyelectrolyte (results not shown), with both LbL architectures (PAH/GO)_n and (PAH/GPSS)_n displaying a linear rise in absorbance with increasing *n*, suggesting that the same amount of material was adsorbed at each deposition step in the LbL film formation.

Figure S4 shows the AFM analysis for the LbL films. (PAH/GO)₅ presented platelets with lateral dimensions ranging from 10 to 30 μm , while it was observed smaller platelets with lateral dimensions ranging from 1 to 5 μm in the (PAH/GPSS)₅ film, as already predicted by I_D/I_G ratio in Raman spectroscopy. The height profile (Figure S4a) displays a large fragment of a wrinkled GO platelet in the film surface ($\sim 50 \text{ nm}$), where apparently all the background surface is covered with thin GO layers, with

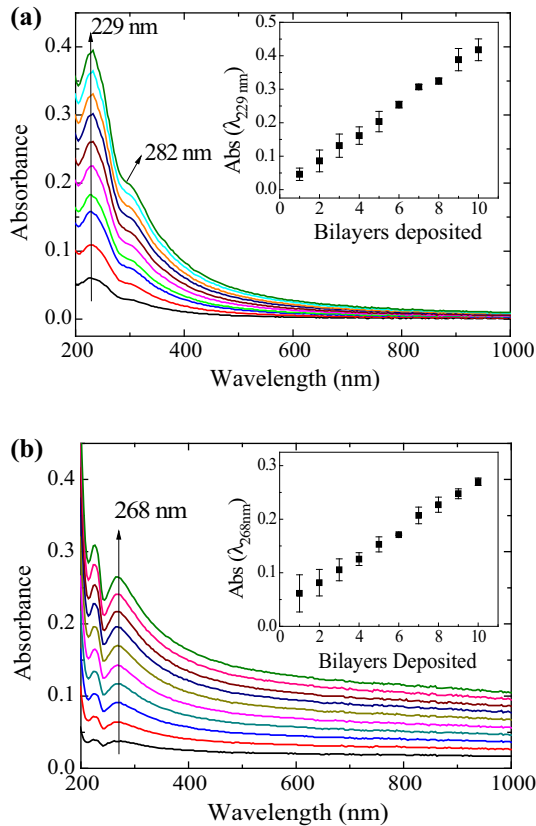


Fig. 5 UV–Vis absorption spectra of the LbL films growth onto quartz plates: **a** (PAH/GO)₁₀; **b** (PAH/GPSS)₁₀.

smaller platelets for GPSS (~ 10 nm height) (see Fig. S4b). LbL film thickness analysis was performed scratching both (PAH/GO)₅ and (PAH/GPSS)₅ films (topography images and height profile shown in Figure S5), indicating an average thickness of ~ 2 nm per deposited PAH/GO bilayer and ~ 4 nm per deposited PAH/GPSS bilayer, reinforcing the rGO wrapping by PSS molecules and also monolayer thickness values comparable to those reported in the literature [57]. The electronic properties of the films were investigated by impedance measurements taken from 1 Hz to 1 MHz (Fig. 6). Figure 6a shows the impedance modulus analysis with (PAH/GO)₅ film presenting a dielectric material profile as expected, with higher impedance in the low-frequency region (> 10⁸ Ω) followed by a capacitive behavior > 100 Hz (see phase angle analysis in Fig. 6b). (PAH/GPSS)₅ LbL film displayed a more conductive behavior with impedance values ~ four times lower than those presented by (PAH/GO)₅.

An increase in the film conductivity is expected with the restorage of the sp² network after the

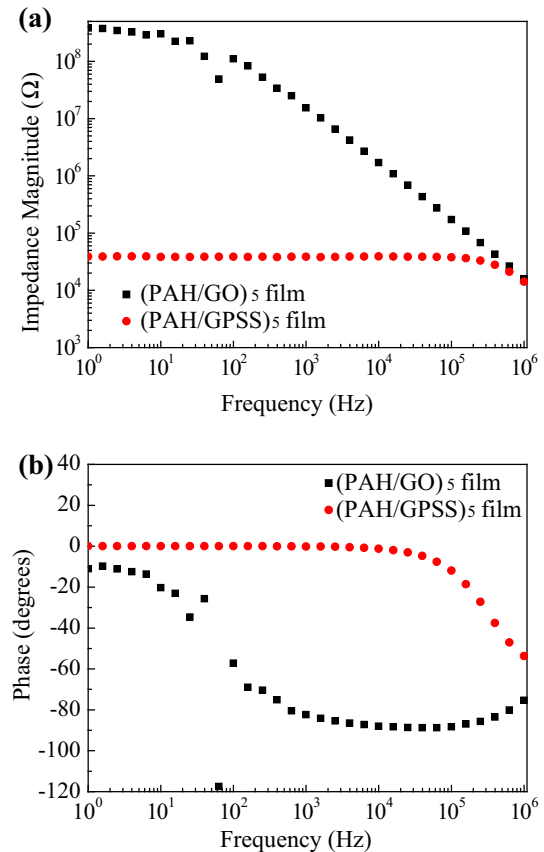


Fig. 6 **a** Impedance modulus and **b** phase angle spectra of (PAH/GO)₅ and (PAH/GPSS)₅ LbL films.

chemical reduction process; however, one must have in mind the formation of defective rGO nanoplatelets wrapped by PSS (insulating material) molecules. GPSS was also alternately deposited with a non-conductive material (PAH) to form multilayered (PAH/GPSS) nanostructures; therefore, a 7000-fold decrease in the overall resistance, from ~ 300 MΩ of (PAH/GO)₅ to 39 kΩ of (PAH/GPSS)₅, respectively, was observed. In a seminal paper, Kotov et al. [58] demonstrated the assembly of (polyelectrolytes/GO) films followed by an in-situ chemical reduction, immersing the LbL (polyelectrolytes/GO) films into aqueous hydrazine solution. They observed a 2700-fold decrease in the overall resistance, changing from 32 MΩ to 12 kΩ after the chemical treatment. Rani et al. [50] fabricated multilayered films using cationic and anionic graphene-based polyelectrolytes that presented 5000 MΩ resistance with six deposited bilayers, which was further dropped to 30 kΩ after 2-h annealing at 250 °C under a nitrogen atmosphere. Kim and Min [59] observed a decrease in the sheet

resistance of graphene oxide layers with the adsorption of multi-walled carbon nanotubes (MWCNTs). A graphene oxide/aminated MWNTs bilayer was self-assembled and chemically reduced by immersion into aqueous hydrazine solution, presenting a sheet resistance of $\sim 1.0 \text{ M}\Omega/\text{sq}$. The film was annealed 1 h at $500 \text{ }^\circ\text{C}$ under argon atmosphere, changing the sheet resistance to $100 \text{ k}\Omega/\text{sq}$. In general, an additional processing (in situ reduction or annealing) is necessary after the LbL film fabrication to achieve $\text{k}\Omega$ -order resistance. Here, that was achieved from aqueous suspensions of GPSS straightforward in the LbL assembly, which can be easily explained by the non-covalent interactions between rGO and PSS molecules, thus enabling a more conductive state to the GPSS nanoplatelets. In addition, this composite material can be easily processed without further processing to tune charge transport and carrier mobility at interfaces [60], highly keen in electronic applications.

Conclusions

The present work demonstrated a successful synthesis of GPSS nanoplatelets that easily form stable water suspensions. MD simulations elucidated the driven force involved in the GPSS formation. The presence of functional groups in the rGO favors physical interactions with the PSS molecules, thus creating a composite, hybrid material with interesting electrical properties. The atomic structure of the materials forming the GPSS structure is essentially attributed to H-bond formation between oxygen groups in PSS with hydrogen from hydroxyl and carboxyl groups in rGO. Those interactions are favored even in the presence of water, forming an interesting system to build up ordered multilayer nanostructures using the LbL assembly. (PAH/GO) and (PAH/GPSS) LbL films displayed a good linear growth, with the GO film presenting larger nanoplatelets when compared to GPSS due to the chemical attack during the chemical reduction in the GPSS formation. The non-covalent interactions between PSS and rGO endow interesting electrical properties to GPSS, which is four orders of magnitude more conductive than GO.

Supplementary material

See supplementary material for UV–Vis, XPS survey and FTIR spectra. Also, AFM morphology images, height profile and E versus i plots.

Acknowledgements

Authors are grateful to FAPESP (2010/13033-6, 2012/01484-9, 2015/14703-9, 2016/00023-9, 2014/24547-1 and 2014/11410-8), INEO (CNPq) for financial support, and also Bernhard Gross Polymer Group (IFSC–USP), Ângelo L. Gobbi and Maria Helena O. Piazzetta at Laboratory of Microfabrication (LNNano/CNPEM) for the cooperation in micro-electrodes fabrication. This research also used the computing resources and assistance of the John David Rogers Computing Center (CCJDR) in the Institute of Physics “Gleb Wataghin,” University of Campinas.

Compliance with ethical standards

Conflicts of interest No conflicts of interest.

Electronic supplementary material: The online version of this article (<https://doi.org/10.1007/s10853-018-2325-1>) contains supplementary material, which is available to authorized users.

References

- [1] Brownson DAC, Kampouris DK, Banks CE (2011) An overview of graphene in energy production and storage applications. *J Power Sour* 196:4873–4885
- [2] Cai H, Li J, Xu X et al (2017) Nanostructured composites of one-dimensional TiO_2 and reduced graphene oxide for efficient dye-sensitized solar cells. *J Alloys Compd* 697:132–137
- [3] Liang B, Guo X, Fang L et al (2015) Study of direct electron transfer and enzyme activity of glucose oxidase on graphene surface. *Electrochem Commun* 50:1–5
- [4] Shao Y, Wang J, Wu H et al (2010) Graphene based electrochemical sensors and biosensors: a review. *Electroanalysis* 22:1027–1036
- [5] Gupta V, Chaudhary N, Srivastava R et al (2011) Luminescent graphene quantum dots for organic photovoltaic devices. *J Am Chem Soc* 133:9960–9963

- [6] Bonaccorso F, Sun Z, Hasan T, Ferrari AC (2010) Graphene photonics and optoelectronics. *Nat Photonics* 4:611–622
- [7] Kholmanov IN, Magnuson CW, Piner R et al (2015) Optical, electrical, and electromechanical properties of hybrid graphene/carbon nanotube films. *Adv Mater* 27:3053–3059
- [8] Novoselov KS, Geim AK, Morozov SV et al (2004) Electric field effect in atomically thin carbon films. *Science* 306:666–669
- [9] Jang J, Son M, Chung S et al (2015) Low-temperature-grown continuous graphene films from benzene by chemical vapor deposition at ambient pressure. *Sci Rep* 5:17955
- [10] Shao J-J, Lv W, Yang Q-H (2014) Self-assembly of graphene oxide at interfaces. *Adv Mater* 26:5586–5612
- [11] Hummers WS, Offeman RE (1958) Preparation of graphitic oxide. *J Am Chem Soc* 80:1339
- [12] Wang G, Shen X, Wang B et al (2009) Synthesis and characterisation of hydrophilic and organophilic graphene nanosheets. *Carbon* 47:1359–1364
- [13] Pei S, Cheng H-M (2012) The reduction of graphene oxide. *Carbon* 50:3210–3228
- [14] Loh KP, Bao Q, Eda G, Chhowalla M (2010) Graphene oxide as a chemically tunable platform for optical applications. *Nat Chem* 2:1015–1024
- [15] Richardson JJ, Bjornmalm M, Caruso F (2015) Technology-driven layer-by-layer assembly of nanofilms. *Science* 348:2491–2491
- [16] Hu J, He B, Lu J et al (2012) Facile preparation of Pt/polyallylamine/reduced graphene oxide composites and their application in the electrochemical catalysis on methanol oxidation. *Int J Electrochem Sci* 7:10094–10107
- [17] Huang C, Li C, Shi G (2012) Graphene based catalysts. *Energy Environ Sci* 5:8848–8868
- [18] Cohen-Tanugi D, Lin L-C, Grossman JC (2016) Multilayer nanoporous graphene membranes for water desalination. *Nano Lett* 16:1027–1033
- [19] Long Y, Wang K, Xiang G et al (2017) Molecule channels directed by cation-decorated graphene oxide nanosheets and their application as membrane reactors. *Adv Mater* 29:1606093–1606097
- [20] Bo X, Zhou M, Guo L (2017) Electrochemical sensors and biosensors based on less aggregated graphene. *Biosens Bioelectron* 89(1):167–186
- [21] Mascagni DBT, Miyazaki CM, da Cruz NC et al (2016) Layer-by-layer assembly of functionalized reduced graphene oxide for direct electrochemistry and glucose detection. *Mater Sci Eng C* 68:739–745. <https://doi.org/10.1016/j.msec.2016.06.001>
- [22] Hsiao S-T, Ma C-CM, Liao W-H et al (2014) Lightweight and flexible reduced graphene oxide/water-borne polyurethane composites with high electrical conductivity and excellent electromagnetic interference shielding performance. *ACS Appl Mater Interfaces* 6:10667–10678
- [23] Lee DW, Hong T-K, Kang D et al (2011) Highly controllable transparent and conducting thin films using layer-by-layer assembly of oppositely charged reduced graphene oxides. *J Mater Chem* 21:3438
- [24] Zou J, Kim F (2014) Diffusion driven layer-by-layer assembly of graphene oxide nanosheets into porous three-dimensional macrostructures. *Nat Commun* 5:5254
- [25] Liu Y, Liu Y, Feng H et al (2012) Layer-by-layer assembly of chemical reduced graphene and carbon nanotubes for sensitive electrochemical immunoassay. *Biosens Bioelectron* 35:63–68
- [26] Marmisollé WA, Azzaroni O (2016) Recent developments in the layer-by-layer assembly of polyaniline and carbon nanomaterials for energy storage and sensing applications. From synthetic aspects to structural and functional characterization. *Nanoscale* 8:9890–9918
- [27] Decher G (1997) Fuzzy nanoassemblies: toward layered polymeric multicomposites. *Science* 277:1232–1237
- [28] Decher G, Hong JD, Schmitt J (1992) Buildup of ultrathin multilayer films by a self-assembly process: III. Consecutively alternating adsorption of anionic and cationic polyelectrolytes on charged surfaces. *Thin Solid Films* 2:831–835
- [29] Kovtyukhova NI, Ollivier PJ, Martin BR et al (1999) Layer-by-layer assembly of ultrathin composite films from micron-sized graphite oxide sheets and polycations. *Chem Mater* 11:771–778. <https://doi.org/10.1021/cm981085u>
- [30] Stankovich S, Piner RD, Chen X et al (2006) Stable aqueous dispersions of graphitic nanoplatelets via the reduction of exfoliated graphite oxide in the presence of poly(sodium 4-styrenesulfonate). *J Mater Chem* 16:155
- [31] Giroto EM, Santos IA (2002) Medidas de resistividade elétrica DC em sólidos: Como efetuá-las corretamente. *Quím Nova* 25:639
- [32] Bagri A, Mattevi C, Acik M et al (2010) Structural evolution during the reduction of chemically derived graphene oxide. *Nat Chem* 2:581–587
- [33] Dreyer DR, Park S, Bielawski CW, Ruoff RS (2009) The chemistry of graphene oxide. *Chem Soc Rev* 39:228–240
- [34] Berendsen HJC, Postma JPM, van Gunsteren WF et al (1984) Molecular dynamics with coupling to an external bath. *J Chem Phys* 81:3684–3690
- [35] Hoover W (1985) Canonical dynamics: equilibrium phase-space distributions. *Phys Rev A* 31:1695–1697
- [36] Martyna GJ, Klein ML, Tuckerman M (1992) Nosé–Hoover chains: the canonical ensemble via continuous dynamics. *J Chem Phys* 97:2635–2643

- [37] Jorgensen WL, Chandrasekhar J, Madura JD et al (1983) Comparison of simple potential functions for simulating liquid water. *J Chem Phys* 79:926–935
- [38] Carrillo J-MY, Dobrynin AV (2010) Detailed molecular dynamics simulations of a model NaPSS in water. *J Phys Chem B* 114:9391–9399
- [39] Jiao S, Xu Z (2015) Selective gas diffusion in graphene oxides membranes: a molecular dynamics simulations study. *ACS Appl Mater Interf* 7:9052–9059
- [40] Martínez L, Andrade R, Birgin EG, Martínez JM (2009) PACKMOL: a package for building initial configurations for molecular dynamics simulations. *J Comput Chem* 30:2157–2164
- [41] Plimpton S (1995) Fast parallel algorithms for short-range molecular dynamic. *J Comput Phys* 117:1–19
- [42] Khanra P, Kuila T, Kim NH et al (2012) Simultaneous bio-functionalization and reduction of graphene oxide by baker's yeast. *Chem Eng J* 183:526–533
- [43] Liu Y, Gao L, Sun J et al (2009) Stable nafion-functionalized graphene dispersions for transparent conducting films. *Nanotechnology* 20:465605
- [44] Jiang G, Baba A, Advincula R (2007) Nanopatterning and fabrication of memory devices from layer-by-layer poly(3,4-ethylenedioxythiophene)–poly(styrene sulfonate) ultrathin films. *Langmuir* 23:817–825
- [45] Pimenta MA, Dresselhaus G, Dresselhaus MS et al (2007) Studying disorder in graphite-based systems by Raman spectroscopy. *Phys Chem Chem Phys* 9:1276
- [46] Ferrari AC, Meyer JC, Scardaci V et al (2006) Raman spectrum of graphene and graphene layers. *Phys Rev Lett* 97:187401
- [47] Wang Y, Alsmeyer DC, McCreery RL (1990) Raman spectroscopy of carbon materials: structural basis of observed spectra. *Chem Mater* 2:557–563
- [48] Yang D, Velamakanni A, Bozoklu G et al (2009) Chemical analysis of graphene oxide films after heat and chemical treatments by X-ray photoelectron and Micro-Raman spectroscopy. *Carbon* 47:145–152
- [49] Pham VH, Cuong TV, Hur SH et al (2010) Fast and simple fabrication of a large transparent chemically-converted graphene film by spray-coating. *Carbon* 48:1945–1951
- [50] Rani A, Oh KA, Koo H et al (2011) Multilayer films of cationic graphene-polyelectrolytes and anionic graphene-polyelectrolytes fabricated using layer-by-layer self-assembly. *Appl Surf Sci* 257:4982–4989
- [51] Wang S, Yu D, Dai L et al (2011) Polyelectrolyte-functionalized graphene as metal-free electrocatalysts for oxygen reduction. *ACS Nano* 5:6202–6209
- [52] Zhang Y, Hu W, Li B et al (2011) Synthesis of polymer-protected graphene by solvent-assisted thermal reduction process. *Nanotechnology* 22:345601
- [53] Lu J, Do I, Fukushima H et al (2010) Stable aqueous suspension and self-assembly of graphite nanoplatelets coated with various polyelectrolytes. *J Nanomater* 2010:11
- [54] Si Y, Samulski ET (2008) Synthesis of water soluble graphene. *Nano Lett* 8:1679–1682
- [55] He P, Derby B (2017) Inkjet printing ultra-large graphene oxide flakes. *2D Mater* 4:021021
- [56] Gross MA, Sales MJA, Soler MAG et al (2014) Reduced graphene oxide multilayers for gas and liquid phases chemical sensing. *RSC Adv* 4:17917–17924
- [57] Zheng Q, Kim J-K (2015) Graphene for transparent conductors—synthesis properties. Springer, New York
- [58] Kotov NA, Dékány I, Fendler JH (1996) Ultrathin graphite oxide-polyelectrolyte composites prepared by self-assembly: transition between conductive and non-conductive states. *Adv Mater* 8:637–641
- [59] Kim Y-K, Min D-H (2009) Durable large-area thin films of graphene/carbon nanotube double layers as a transparent electrode. *Langmuir* 25:11302–11306
- [60] Jimenez MJM, Oliveira RF, Almeida TP et al (2017) Charge carrier transport in defective reduced graphene oxide as quantum dots and nanoplatelets in multilayer films. *Nanotechnology* 28:495711